Failure Probabilities of Ferritic Spent-Fuel Casks Subjected to Real Accident Events

P. McConnell[1], A.H. Sanders[1], J.W. Jones[2], R.E. Nickell[3], R.F. Williams[4]

[1]*General Research Corporation, Santa Barbara, California*

[2]*Swanson Service Corporation, Huntington Beach, California*

[3]*Applied Science & Technology, Poway, California*

[4]*Electric Power Research Institute, Palo Alto, California, United States of America*

This paper discusses an assessment (McConnell et al. 1988), of the probability of breach of containment, which may result in the release of radioactive material, from ferritic spent-fuel transport casks subjected to severe accidents. A motivation for such an analysis is to evaluate the dual-purpose application for ferritic casks which are presently being used to store spent-fuel and which may have some economic advantage over traditional stainless steel casks (Casper et al.).

Regulations require the transport cask applicant to demonstrate that the structural containment of a cask can withstand a sequence of hypothetical accident events including a thirty-foot drop onto an unyielding surface and a forty-inch drop onto a mild steel pin. Existing spent-fuel casks licensed for transport are all of a sandwich design employing a thin stainless steel containment boundary and a lead or depleted uranium shield (Johnson and Notz). The margin of safety of these casks, particularly for severe, or extra-regulatory events, may be the basis by which cask designs constructed of alternative materials are ultimately evaluated (Barrett).

The ferritic construction materials for the alternative cask designs, forged steel and ductile cast iron, differ from the conventional austenitic stainless steel casks used for Type B transport packagings. Ferritic materials (as well as the titanium alloys under consideration for cask body application) are subject to brittle fracture, especially at service temperatures near or below the nil-ductility transition temperature when subjected to high stresses and/or when large pre-service or service-induced flaws are present.

The assessment of the ferritic spent-fuel casks was based upon probabilistic fracture mechanics. Fracture mechanics provides a means for predicting brittle fracture by relating the stresses which may be applied to a component (say, due to accidents) and the inherent flaws contained in the component, with the component material's resistance to crack initiation ("fracture toughness"). Probabilistic representation of these parameters allows for a quantitative prediction of the probability of crack initiation in a given component.

CASK DESIGNS / MATERIALS

Two large (117 ton) 21 PWR assembly rail casks of thick-wall monolithic design, similar except that one was assumed to be constructed of ferritic steel, the other ferritic ductile iron, were analyzed. The steel cask was 191 inches in length with an 88 inch outer diameter, and a 12.94 inch wall; the ductile iron cask was 192 inches long, 90 inches in diameter, and had a 14 inch wall.

The ductile iron material properties were based upon those of existing ductile iron casks (McConnell and Lombrozo) and an ASTM specification (A874) for ductile iron. The fracture toughness of the ductile iron was chosen to be a nominal 60 ksi-in$^{1/4}$. The ferritic steel was assumed to be ASTM A508-4 with a nominal fracture toughness of 120 ksi-in$^{1/4}$. The assumed yield and tensile strengths of the ductile iron were 30 ksi and 49.5 ksi, respectively, with an 11% elongation. The corresponding values for the ferritic steel were 85.5 ksi, 132 ksi, and 16.5%.

The closure system in both casks was a thick, double-step stainless steel lid attached to the cask body with a large number of closely spaced bolts. The limiters were assumed to be constructed of wood with known elastic-plastic load-deflection properties.

STRESS ANALYSES

Finite-element stress analyses were performed on each spent-fuel cask design to determine the actual stresses associated with the regulatory design-basis loading event. The finite element codes ANSYS^{R} and PRONTO-2D were used. An elastic analysis of each cask was performed for six drop orientations, β: 0°, 10°, 70°, 90°, 250°, and 270°. The analyses assumed the cask was dropped from thirty-feet onto a flat unyielding surface. The stresses calculated for this event were the basis from which stresses associated with all other drop heights, targets, and/or orientations were derived for the probabilistic analyses by ratioing or "scaling" the deceleration resulting from a given accident scenario to that from the thirty-foot drop onto the unyielding surface.

Stresses for up to 580 "volumes" in the cask body were input into the probabilistic analysis code for each of the six drop orientations. The stress was assumed to be constant over the entire volume associated with the point chosen for reporting. The highest calculated stresses for each drop orientation were always included for evaluation. Stresses were interpolated for different drop orientations. The stress values used were the "stress intensity" defined as the absolute value of the difference between the maximum and minimum principal stress at a given location. This very conservatively assumes tensile stress throughout the cask body; in actual fact large compressive regions may be expected to exist.

Rigid Body Analysis

This analysis determined the maximum deceleration which would be experienced by the casks impacting in several orientations. The impact was modeled as a rigid body quasi-static problem in which all the drop energy at impact was absorbed by permanent deformation of the cask limiter. Initial impact velocities assumed ranged from 10 to 150 ft/s. Uniform decelerations calculated for the 30-foot drop height design-basis analyses (44ft/s), ranging from 90 g to 118 g depending upon the drop orientation, were used to obtain the stress distribution in the cask for each orientation.

Stress Distribution

An ANSYS analysis was performed for each drop orientation to determine the stress distribution in the cask bodies for a uniform deceleration calculated for the 30-foot drop design-basis analysis. Boundary conditions were applied to the casks as follows:

End Drop

Symmetry of the cask, when loaded in the longitudinal axis, allowed for use of a wedge-shaped model. Static deceleration was applied in small increments until the limiter deflected into the final configuration. The contents of the cask were conservatively modeled by increasing the material density to account for the additional content weight.

Side Drop/Corner Drop/Slap-Down

The side-drop and corner-drop stress analyses utilized a full 180° finite element model. The limiter was modeled using one-dimensional springs to ground. The deceleration of the cask was applied as an equivalent global deceleration loading in the vertical direction. The contents of the cask were modeled by increasing the density of the cask materials. The cask lid was conservatively modeled as being supported only at 135° around the bottom side of the cask wall and assuming a frictionless sealing surface. The slap-down analysis was performed much like the corner drop analyses except that an additional loading technique was necessary to introduce the rotational inertia of the cask into the evaluation.

Dynamic Analysis of Lid

The lid was modeled using ANSYS nonlinear transient dynamic analysis capabilities that simulate the impact deceleration and allow for separation at the sealing interface and inelastic deformation of the bolts if the yield stress is exceeded. For decelerations below the equivalent static load capacity of the bolts, it was found that the gap between the head and body remained closed. When the deceleration reached approximately 175 g's, the bolts were found to exhibit permanent plastic strain which could result in release of radioactive contents. There is a very narrow range of deceleration values between where completely elastic bolt response occurs and the bolts experience sufficient plasticity to overcome the elastic preload.

Non-Linear Material Effects

The stresses were calculated for a thirty-foot drop with acceleration loads based upon the rigid body analysis of the impact limiters. At increased impact velocities and acceleration loads, stresses will exceed the yield point of the material at certain locations resulting in stress redistribution. The maximum stresses will remain at the yield point, modified by the accumulated plastic strains. Scaling the elastically-calculated stresses results in highly unrealistic stresses for high accelerations, and unrealistic estimates of the applied stress intensity and the propensity to fracture.

The conservatism inherent in assuming a linear relationship between stress and acceleration was evaluated by making a comparison of the elastically-calculated stresses to the plastically-calculated stresses in the cask for impacts of the same severity. PRONTO-2D was used to calculate the elastic-plastic stress distribution in the cask for an end drop. The stress distribution in the cask was very similar at the inside and outside surfaces for both the elastic and elastic-plastic analyses, i.e., the effect of stress redistribution is minimal. Limiting the stresses to near yield with the equivalent-elastic strain model employed, and assuming only tensile stresses, was a conservative approach to characterize the stress distribution for the probabilistic analysis.

PROBABILISTIC ANALYSIS

Accident Scenarios

Rail accident scenarios identified by Fischer et al. were employed. The schematic representation of an accident is shown in Figure 1. Each accident scenario has a specific surface hardness (h), and probability distributions for cask orientation (β), impact angle (α), and accident velocity (v).

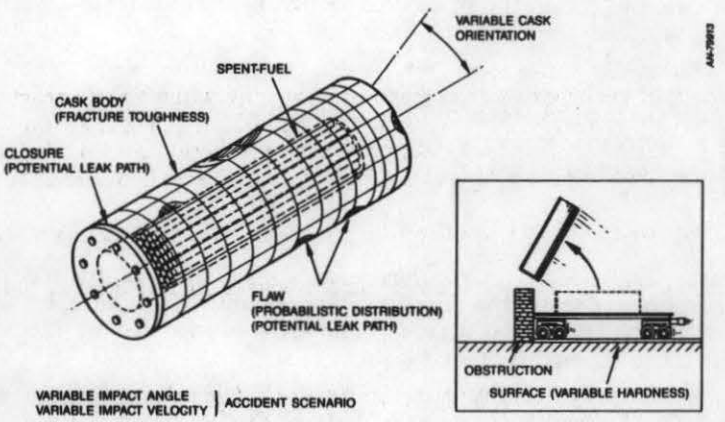

Figure 1. Spent-Fuel Cask and Accident Scenario Variables.

Stress Scaling

The stress analyses computed the deceleration and the stress distributions in the cask for regulatory conditions. Stresses for a given accident scenario were obtained by multiplying the stresses under regulatory conditions by the "scale factor" ratioing the deceleration to be expected for the particular accident conditions (v, α, β, h). The relationship between deceleration and impact velocity was determined, based upon the effectiveness of the impact limiters, at each orientation angle for which the stresses were calculated and for the surface hardness levels encountered in the accident scenarios.

Equivalent-Elastic Strain Model

The ANSYS finite-element stress analyses generated elastic stresses. The elastic stresses, adjusted by the stress scaling procedure, often resulted in prediction of stresses greater than the yield strength of the cask body. In order to mitigate the large conservatism associated with using post-yield elastically-calculated stresses in the probabilistic model, without resorting to performing expensive

plastic stress analyses, an equivalent-elastic strain model was adopted. This model assumes that the energy associated with a particular loading event, as calculated from an elastic stress analysis, is equivalent to the energy absorbed should plastic deformation occur. Therefore, the area under the elastic stress curve can be compared with that under the true stress/strain curve which accounts for yielding of the cask body. This procedure results in a lowering of the stress for a given loading event and an increase in the predicted strain. This stress was then used in the linear-elastic fracture mechanics calculation to predict crack initiation.

Computational Procedure

The computational flow chart for computing the probability of cask failure due to crack formation and/or lid failure is shown in Figure 2.

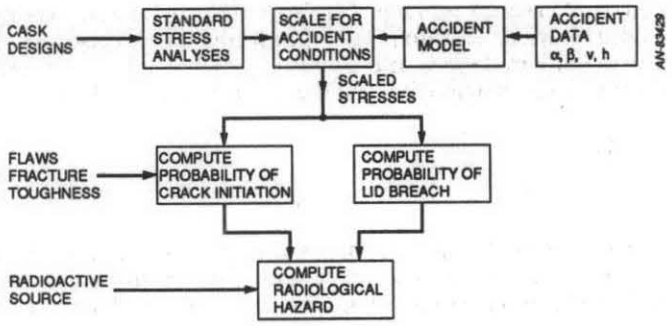

Figure 2. Probabilistic Analysis Flow Chart.

Failure Mechanisms

"Failure" of the spent-fuel cask body was defined as occurring when brittle fracture initiates from a preëxisting flaw. This is a conservative assumption because i) a crack may not initiate in a brittle manner, but rather ductile initiation and stable tearing may occur, and ii) the crack may arrest in the compressive stress regions before it would extend through the wall of the cask.

When the ductility limit was exceeded, ductile rupture of the cask body was assumed to occur.

Additionally, leakage was assumed around the lid seals above a critical level of loading of 175 g.

Radiation Release

The source term and the total radioactive material available for release was the same as assumed by Fischer et al. Discussion of the mechanisms for and quantification of radioactive material release and gamma radiation exposure is given elsewhere (McConnell et al. 1988).

Variables Affecting Probabilistic Analyses

Flaw Parameters

The flaws were assumed to be crack-like semielliptical surface flaws with the length to depth ratio of 6:1. The flaws were assumed to be oriented normal to the maximum applied tensile (crack-opening) stresses. A nominal flaw density of one defect per 10,000 cubic inches of cask body was assumed, representing 60 to 70 flaws in the approximately 700,000 inch^3 cask volume.

The inherent distribution of flaw depths, P_a, was treated probabilistically:

$$P_a = \exp(-a/\mu) / \mu[1 - \exp(-h/\mu)]$$

where μ = mean flaw size (variable, nominally 0.246 inch), a = flaw depth, and h = wall thickness.

The cask rejection flaw size, a*, is that size defect that, if detected in the cask body during nondestructive examination, would mandate rejection of the cask or repair of the cask body. The rejection flaw size, in practice, should be based upon realistic assessments of flaw detectibility limits and the flaw size considered tolerable in terms of cask integrity. This parameter was varied about a

nominal value of 0.4 inch. The probability of non-detection, P_{ND}, of flaws was based upon an error function nondetection probability:

$$P_{ND} = \tfrac{1}{2}\text{erfc}[1.6\ \ln(a/a_D)]$$

where a_D = crack depth which has 50% probability of detection.

The flaw size a_D, considered variable, was set at a nominal value of 1.25 inches on the basis of conservative estimates (Zhang et al.).

Resultant Flaw Size Distribution

After inspection, the distribution of flaw depths in the cask body is dependent upon the inherent distribution P_a and the probability of non-detection P_{ND}. Below a*, the distribution is P_a since even if flaws are detected, the cask is not rejected. Above a*, the probability of having a flaw is the probability of not detecting it given that it existed in the first place. The probability distribution for that region is therefore the product of P_a and P_{ND}.

Fracture Toughness, K_{Id}

Fracture toughness is the material property that provides resistance to initiation of a crack from a preëxisting defect under application of stress. A Gaussian distribution for the dynamic fracture toughness values was assumed with a 10% standard deviation about the mean.

Probabilistic Fracture Mechanics

Brittle crack initiation occurs when the applied stress intensity (K_I) on a flaw exceeds the critical stress intensity (K_{Id}). The expression used for K_I was:

$$K_I = 1.13\sigma\sqrt{(\pi a)}\ [1 - 0.08(a/c)]\ [1 + 1.464(a/c)^{1.65}]^{-\frac{1}{2}}$$

where σ = stress and 2c = flaw length.

Since the flaw depth and applied stresses were random variables, K_I is a random variable whose probability distribution is obtained from the distribution for flaw depth for a given stress. The probability of an existing flaw causing failure, PF, is the probability of the stress intensity on the flaw, K_I, being greater than the fracture toughness, K_{Id}. The mathematical procedures for calculating the probability that K_I exceeds K_{Id}, and therefore that brittle crack inititation occurs, is given in McConnell et al. 1988.

If we assume that the number of flaws in a volume, V, has a Poisson distribution with a mean, λ, then the probability that a failure will occur in a given volume is given by expression for Poisson distributions:

$$P_{fail} = 1 - \exp[-\lambda VPF]$$

The probabililty of failure for the entire cask is computed from the individual probabilities of failure by:

$$\begin{aligned}\text{Pcaskfail} &= 1 - (\text{probability that none of the volumes fail}) \\ &= 1 - (1\text{-pfail}_1) * (1\text{-pfail}_2) * \ldots * (1\text{-pfail}_n)\end{aligned}$$

where n = number of volumes in the cask.

Incorporation of Accidents

The risk resulting from all accident scenarios is quantified by the probability of cask failure and the probability of lid failure. The computation of failure was made for each set of conditions (α, β, v, hardness). The overall value of failure was then computed the over entire range of conditions and for all accident scenarios.

FAILURE PROBABILITIES

Results of the calculations of the probability for breach of containment of the spent-fuel casks

analyzed are reported in terms of variables directly affecting the potential for failure. A set of these probabilistic parameters was selected as a realistic, though conservative representation and varied to determine their affect on the probability of breach of containment given that an accident occurs. In the figures, note the relatively high probability for breach of the closure, P_{lid}, compared to the potential for fracture of the cask body, P_f.

Effect of Rejection Flaw Size (a*) & Inspection Reliability (a_D)

This analysis shows the simultaneous effect on P_f, when varying both the rejection flaw size, a*, and the effectiveness of flaw inspection, defined in terms of the flaw size, a_D. The rejection flaw size, particularly when chosen to be a relatively small value such as 0.4 inch, encourages improved manufacturing practice so that expensive casks are not rejected. The advantage of improved ultrasonic inspection and/or fabrication is apparent. Figure 3 suggests a significant decrease in P_f when either the rejection flaw size and/or a_D are reduced from 2.0 inches to 0.4 inches. The improvement in P_f with decreasing a_D is not so marked for smaller rejection flaw sizes, on the order of 0.2 inches, however, because even the improved inspection procedures have relatively low probability of detecting very small flaws. (The practicality of rejecting a cask on the basis of very small defect sizes is questionable in any event). There is also no advantage of improved inspection when the rejection flaw size is a large as 2.0 inches. Reducing both a_D and a* simultaneously results in maximum benefit.

Effect of Cask Body Fracture Toughness

This analysis shows the effect the cask body material quality has on the potential for failure. Increased fracture toughness results in a decrease in the probability of cask body failure, Figure 4. Increasing the fracture toughness of the ductile iron cask from 60 ksi-in$^{\frac{1}{2}}$ to a 80 ksi-in$^{\frac{1}{2}}$ lowers P_f by a factor of 66. Similar improvements in the P_f for the ferritic steel cask were noted with increasing fracture toughness.

Effect of Limiting Accident Velocities

These analyses will show the benefit to be achieved by limiting the velocity of the train and thereby reducing the maximum stresses to which the cask would be subjected. There are several accident scenarios, however, for which control of velocity is not feasible, such as when a train derails off from a bridge. Such scenarios can be eliminated by route control, however.

Limit Train Velocity, No Route Control

This analysis shows the effect of limiting the train velocity without route control. Little benefit in risk reduction is possible since there are accident scenarios for which velocity control is impossible and which result in severe stresses which dominate the overall probability of failure, Figure 5.

Limit Train Velocity, Route Control

Figure 5 also shows the advantage of limiting the train velocity when there is administrative route control of the train. The route control ensures that the maximum velocity of the cask will not exceed the limit of the train itself. The risk reduction is dramatic: the probability of failure is reduced over two orders of magnitude when a velocity of 30 miles/hour is imposed on the train carrying a ductile iron cask over the P_f expected if no velocity controls were imposed. This risk reduction is over six orders of magnitude if a 20 miles/hour limit is used. It is clear that the concept of route control has immense implications in terms of risk reduction.

High-Integrity Impact Limiters

Mitigation of the risk of breach of containment may be accomplished by reducing the loads to the cask. An effective means to accomplish load reduction is by using high-integrity impact limiters which encase the cask during transport (Haelsig et al.). Results of stress and probabilistic analyses which modeled such an impact limiting system indicate dramatic reductions in risk to both the cask body and closure system approaching two orders of magnitude. With the high-integrity impact limiter, ferritic casks can be designed and operated to have comparable levels of risk as the stainless steel cask designs.

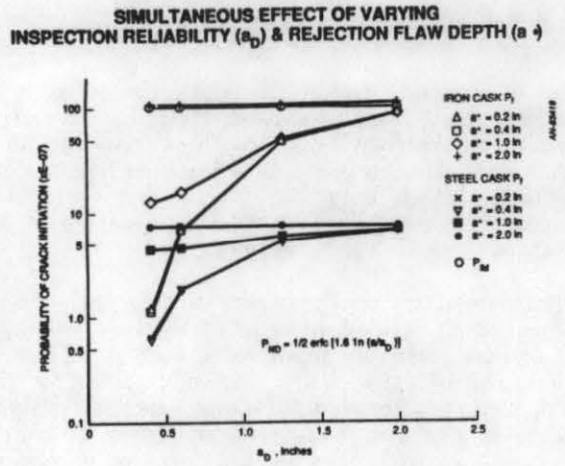

Figure 3. Effect of NDE Reliability (a_D) & Rejection Size (a^*) on P_f.

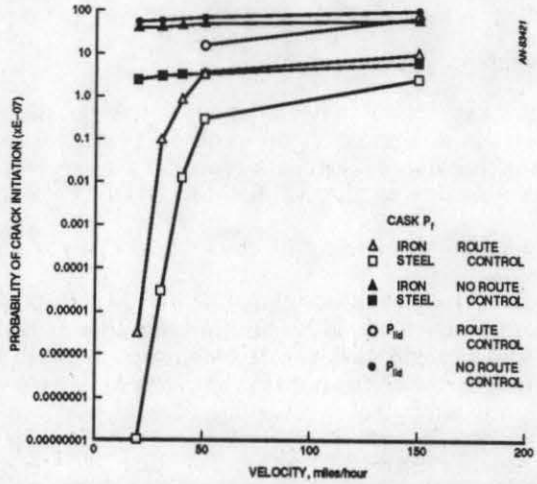

Figure 4. Effect of Improved Cask Body Fracture Toughness on P_f.

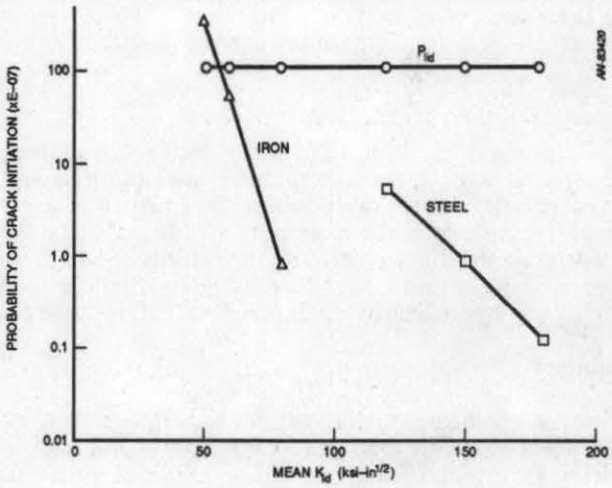

Figure 5. Effect of Limiting Train Velocity on P_f.

CONCLUSIONS

Based upon a realistic, though conservative set of inputs, the probability of fracture of a ductile iron spent-fuel rail cask body, given that an accident occurs, is on the order of 5×10^{-6}. The corresponding probability for a higher toughness ferritic steel cask is approximately 5×10^{-7}. However, these levels of risk are overshadowed by a dominant risk of breach of the closure, approximately 1×10^{-5}, Figure 6.

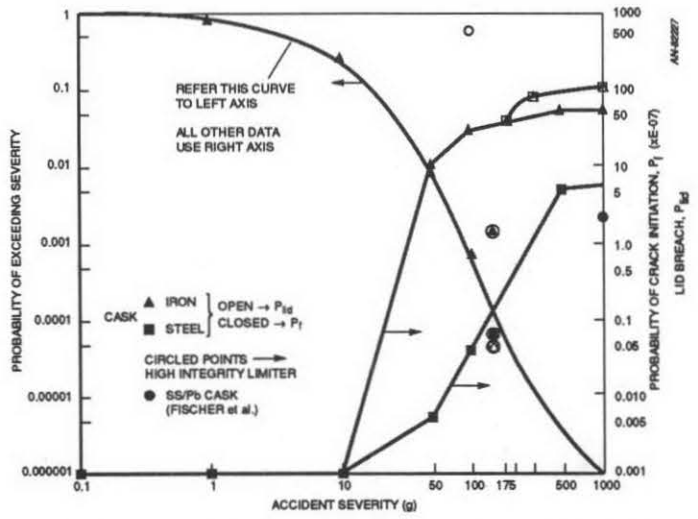

Figure 6. Effect of Accident Severity on P_f and P_{lid}.

Several achievable technical improvements can be implemented to reduce these risk levels by orders of magnitude, including improving the cask body material fracture toughness, more reliable flaw inspection procedures, and, more significantly, utilizing high-integrity impact limiters and/or imposing velocity and route controls on the train carrying the cask.

Stainless steel casks were similarly analyzed (Fischer et al.). The probability of failure of the cask body due to ductile rupture was reported to be about 2×10^{-7}. However, the stainless steel cask system, less robust than the thick-walled monolithic casks, has a high risk of breach of the closure, approximately 6×10^{-4}, nearly fifty times greater than than risk of closure breach calculated for the monolithic casks, Figure 6.

REFERENCES

Barrett, L.H., "Private Industry Opportunity and Challenge: Participation in the DOE/NWPA Transportation Program", AIF Fuel Cycle Conference, (1986).

Brodnick, D.A., "The Utility Industry's Perspective on OCRM's Plans for Developing the System for Transporting Spent Fuel Under the Nuclear Waste Policy Act", for Nuclear Transportation Group, (1987).

Casper, R.M., et al., "Evaluation of Potential Benefits of Transportable Storage Casks", EPRI Report RP2717-08, (1988).

Fischer, L.E., et al., "Shipping Container Response to Severe Highway and Railway Accident Conditions", Lawrence Livermore National Laboratories Report, NUREG/CR-4829, (1987).

Haelsig, R.T., et al., "Conceptual Design of a High-Integrity Impact Limiter for Dual Purpose Cask Rail Transport", EPRI Report RP2813-11, (1989).

Johnson, E.R. and Notz, K.J., "Shipping and Storage Cask Data for Spent Nuclear Fuel", Oak Ridge National Laboratories Report ORNL/TM-11008, (1988).

McConnell, P. and Lombrozo, P., "Ductile Iron Data Base - Correlations Between Microstructure and Fracture Toughness", Sandia National Laboratories Report SAND86-7136, (1987).

McConnell, P., et al., "Probabilistic Analyses of the Response of Alternative Material Monolithic Spent-Fuel Casks Subjected To Real Accident Events", EPRI Report RP2813-06, (1989).

Zhang, Y., et al., "Ultrasonic Inspection of Nodular Cast Iron", EPRI Report RP2813-02, (1988).